

Thermal Infrared 3–5 μm Colors of Obscured and Unobscured Active Galactic Nuclei

Masatoshi Imanishi ^{1,2}

National Astronomical Observatory, Mitaka, Tokyo 181-8588, Japan

ABSTRACT

Thermal infrared photometry in the L - and M' -band and $L - M'$ colors of type-1 and type-2 active galactic nuclei (AGNs) are presented. After combining our observations with photometric data at similar wavelengths taken from the literature, we find that the excess of $L - M'$ colors of type-2 AGNs (37 sources, 50 data points) relative to type-1 AGNs (27 sources, 36 data points), due to dust extinction, is statistically detectable, but very small. We next investigate the $L - M'$ colors of type-2 AGNs by separating less dust-obscured type-2 AGNs and highly dust-obscured type-2 AGNs. In both cases, the $L - M'$ colors are similar to the intrinsic $L - M'$ color of unobscured AGNs, and the $L - M'$ color excess of the latter highly dust-obscured type-2 AGNs due to dust extinction is much smaller than that expected from the Galactic dust extinction curve. Contamination from starbursts and the time lag of flux variation are unlikely to explain this small $L - M'$ color excess, which is best explained if the dust extinction curve in the close vicinity of AGNs is fairly flat at 3–5 μm as a result of a size increase of the absorbing dust grains through coagulation.

Subject headings: galaxies: active — galaxies: nuclei — infrared: galaxies

¹Institute for Astronomy, University of Hawaii, 2680 Woodlawn Drive, Honolulu, Hawaii 96822, USA

²Visiting Astronomer at the Infrared Telescope Facility which is operated by the University of Hawaii under contract to the National Aeronautics and Space Administration.

1. Introduction

According to the current unification paradigm for active galactic nuclei (AGNs), type-1 AGNs (which show broad optical emission lines) and type-2 AGNs (which do not) are intrinsically the same, but the nuclei of the latter class are obscured by dust that lies along our line of sight in dusty molecular tori close to the AGNs (Antonucci 1993). Estimation of the amount of dust along our line of sight in type-2 AGNs and comparison with the amount in type-1 AGNs is an important observational test of the unification paradigm. A direct estimate of dust extinction toward highly luminous type-2 AGNs is necessary to answer the question “how common are highly luminous and highly dust-obscured AGNs (so-called type-2 quasars)?” (Halpern, Turner, & George 1999).

X-ray spectroscopic observations of type-2 AGNs imply higher X-ray absorption columns than do observations of type-1 AGNs, supporting the unification paradigm (e.g., Nandra & Pounds 1994, Smith & Done 1996). However, X-ray absorption is caused both by dust and gas. Estimating the amount of dust along our line of sight (A_V) from X-ray absorption (N_H) is uncertain, since the N_H/A_V ratios toward AGNs are found to vary by more than an order of magnitude (Alonso-Herrero, Ward, & Kotilainen 1997).

For several reasons, we would expect study in the thermal infrared (3–5 μm) wavelength range to be a powerful tool for estimation of dust extinction toward AGNs. Firstly, flux attenuation in this band is purely caused by dust extinction, and the effects of dust extinction are wavelength dependent in the Galactic diffuse interstellar medium (Rieke & Lebofsky 1985, Lutz et al. 1996). Secondly, the absolute flux attenuation by dust extinction is smaller than at shorter wavelengths (Rieke & Lebofsky 1985, Lutz et al. 1996). Thirdly, extended stellar emission generally dominates over obscured AGN emission at $<2 \mu\text{m}$, whereas at $>3 \mu\text{m}$ moderately luminous obscured AGNs show compact, AGN-related emission that dominates observed fluxes (Alonso-Herrero et al. 1998, 2000, Simpson 1998a, but see Simpson, Ward, & Wall 2000). Finally, since the compact emission at 3–5 μm most likely originates in hot (600–1000 K) dust at a part of the dusty molecular torus very near to the AGN (close to the innermost dust sublimation region), the dust extinction toward the 3–5 μm emission region is almost the same as that toward the central engine itself. Hence, by comparing observed continuum fluxes at more than one wavelength between 3 and 5 μm , we can estimate dust extinction toward obscured AGNs directly, up to high magnitudes of obscuration, without serious uncertainties in the subtraction of stellar emission. Some attempts to estimate dust extinction toward obscured AGNs have been made based on near-infrared 1–5 μm colors (Simpson 1998a, Simpson, Rawlings, & Lacy 1999, Simpson et al. 2000), but, given that only upper limits are available at 3–5 μm in most cases, the estimate depends heavily on data at $<3 \mu\text{m}$ in the rest-frame, where stellar emission

dominates the observed fluxes.

We have conducted L ($3.5\pm 0.3 \mu\text{m}$) and M' ($4.7\pm 0.1 \mu\text{m}$) band photometry of type-1 and type-2 AGNs. The main aim is to investigate the $L - M'$ colors of a large number of type-1 and type-2 AGNs and to examine the question of whether $L - M'$ colors are a good measure of the dust extinction toward AGNs. Throughout this paper, $H_0 = 75 \text{ km s}^{-1} \text{ Mpc}^{-1}$, $\Omega_M = 0.3$, and $\Omega_\lambda = 0.7$ are adopted.

2. Target Selection

The target sources were selected based on their proximity and high optical [OIII] emission line luminosities. The first and second criteria were adopted, respectively, to make detection at M' feasible and to select reasonably luminous AGNs (Simpson 1998b), for which contamination from extended star-formation-related emission (both stellar emission and dust emission powered by star-formation activity) is expected to be smaller than it would be for less luminous AGNs. Our samples are heterogeneous and not statistically complete, but provide useful information on the $L - M'$ colors of AGNs.

3. Observation and Data Analysis

L ($3.5\pm 0.3 \mu\text{m}$) and M' ($4.7\pm 0.1 \mu\text{m}$) band photometry was performed at the NASA Infrared Telescope Facility (IRTF) using NSFCAM (Shure et al. 1994). Table 1 gives details of the observations. Sky conditions were photometric throughout the observing runs. The seeing sizes measured from standard stars were $0''.6$ – $1''.2$. The NSFCAM used a 256×256 InSb array. For M' -band photometry, the smallest pixel scale ($0''.06 \text{ pix}^{-1}$) was used during all the observing runs. For L -band photometry, the pixel scale of $0''.06 \text{ pix}^{-1}$ was used in November 1999, while that of $0''.15 \text{ pix}^{-1}$ was used in April and May 2000. The field of view is $14'' \times 14''$ and $38'' \times 38''$ in the case of $0''.06 \text{ pix}^{-1}$ and $0''.15 \text{ pix}^{-1}$ pixel scales, respectively. Each exposure was 0.3–0.4 sec long at L and 0.12–0.2 sec at M' . A dithering technique was utilized with an amplitude of 3– $10''$ to place sources at five different positions on the array. At each dithering position, 50–200 frames were coadded. Offset guide stars were used whenever available to achieve high telescope tracking accuracy.

Standard data analysis procedures were employed, using IRAF³. Firstly, bad pixels

³ IRAF is distributed by the National Optical Astronomy Observatories, which are operated by the Association of Universities for Research in Astronomy, Inc (AURA), under a cooperative agreement with

were removed and the values of these pixels were replaced with interpolated values from the surrounding pixels. Secondly, the frames were dark-subtracted and then scaled to have the same median pixel value, so as to produce a flat frame. The dark-subtracted frames were then divided by a normalized flat frame to produce images at each dithering position. Standard stars and very bright AGNs were clearly seen in images at each dithering position, and so images that contained these were aligned to sub-pixel accuracy using these detected sources and then summed to produce the final images. However, for fainter AGNs, the sources were not always clearly recognizable in the individual images at each dithering position. In these cases the images were shifted based on the records of telescope offset, assuming that telescope pointing and tracking were accurate, and were then summed to produce final images. This procedure potentially broadens the effective point spread function in the final image, providing larger source full widths at half maximum (FWHMs) than the expected values.

At 3–5 μm , and particularly at M' , thermal emission from a small amount of occasionally transiting cirrus can increase sky background signals and affect data quality, even though the sky may look clear. Thus, before summing the frames, we confirmed that their sky background levels agreed to within 1%, showing that the data were not seriously affected by this kind of cirrus.

The images of all the observed AGNs were spatially compact, with no clear extended emission found at either band. The measured FWHMs of some AGNs in the final images were slightly larger than the FWHMs of standard stars, but we attribute these larger FWHMs mainly to the uncertainty introduced by shifting and adding frames containing faint sources, as discussed above. Photometry was done with 6'' diameter apertures, by using the task “PHOT”. Since the 3–5 μm emission was compact, the resulting photometric magnitudes were almost independent of aperture size as long as the aperture sizes were sufficiently larger than the measured FWHMs. Flux calibrations were made by using standard stars in the faint Elias standard star catalog ⁴ or IRTF bright infrared standard star catalog ⁵. The M' -band magnitudes of standard stars were assumed to be the same as the M -band magnitudes listed in these catalogs, because the $M - M'$ color is expected to be virtually 0 mag unless a standard star is of a very late type.

M' -band photometry is inherently very difficult because of the large background noise. The photometric accuracy was strongly dependent on the uncorrectable spatial fluctuation

the National Science Foundation.

⁴ http://irtf.ifa.hawaii.edu/online/IRTF/Catalogs/Elias_standards

⁵ http://irtf.ifa.hawaii.edu/online/IRTF/Catalogs/bright_standards

of background signals; because of this uncorrectable fluctuation, M' -band photometric accuracy was not necessarily better in objects with longer integration time. Furthermore, since the smallest pixel scale ($0''.06 \text{ pix}^{-1}$) had to be utilized in our observations to avoid saturation, emission from the compact AGN emission was spread over many pixels, which made the recognition of real detections even more difficult. To avoid spurious detections, we divided M' -band data into two or three independent images and confirmed that the source positions agreed with each other.

4. Results

Our new photometric measurements for type-1 and type-2 AGNs are tabulated in Table 2. We estimate $L - M'$ colors based on L - and M' -band photometric data taken on the same night or two successive nights. Figure 1a shows the distribution of $L - M'$ colors of the AGNs measured with our standard $6''$ diameter apertures. Based on photometry of quasars (at $<2.2 \mu\text{m}$, $3.7 \mu\text{m}$, and $10.1 \mu\text{m}$), Neugebauer et al. (1987) found that the continuum spectral energy distribution can be approximated by a power law of the form $F_\nu \propto \nu^{1.4 \pm 0.3}$ at $3\text{--}5 \mu\text{m}$, which implies that the intrinsic $L - M'$ color of quasars is 1.0 ± 0.1 . Since this color was derived using quasars (that is, highly luminous unobscured AGNs), any contamination from star-formation-related emission is expected to be very small. We adopt this value for the intrinsic $L - M'$ color of unobscured AGNs. The type-1 and type-2 AGNs in Figure 1a both show $L - M'$ colors similar to the intrinsic $L - M'$ color of unobscured AGNs.

To increase the sample size, we search the available literature for $3\text{--}5 \mu\text{m}$ photometric data on galaxies. Table 3 summarizes the results for sources whose magnitudes have been measured both at $\sim 3.5 \mu\text{m}$ (L - or L' -band) and at $\sim 4.7 \mu\text{m}$ (M' - or M -band). We exclude sources for which only upper limits were given at one wavelength. When photometry has been performed with several different aperture sizes by the same authors, we have tabulated the photometric results based on the smallest aperture, in order to minimize contamination from the extended star-formation-related emission of the host galaxies, except in the case of NGC 1068, for which photometry with a $0''.6$ aperture was adopted (Marco & Alloin 2000). The aperture sizes used are $0''.6\text{--}22''.5$. The central wavelength and wavelength coverage of the filters used for photometry at these two bands differ slightly among authors, and magnitude conversion formulas between slightly different filters are not well established. We therefore assume that photometric magnitudes in slightly different filters are the same. Although this assumption might introduce an uncertainty in the final photometric magnitudes of 0.1 mag or so, this would not affect our conclusions. Figure 1b plots $L - M'$

colors of these AGNs and starburst/LINER galaxies taken from the literature.

5. Discussion

5.1. Comparison of $L - M'$ Colors

After combining our data with data in the literature, we find that, for type-1 AGNs (27 sources, 36 data points), type-2 AGNs (37 sources, 50 data points), and starbursts/LINERs (22 sources, 23 data points), the median (mean) $L - M'$ colors are 0.9 (0.8), 0.9 (1.0), and 0.4 (0.3) respectively. The median $L - M'$ colors of both type-1 and type-2 AGNs are within the range of the intrinsic $L - M'$ color of unobscured AGNs (1.0 ± 0.1), but that of starbursts/LINERs is clearly smaller than those of AGNs. Since the relative contribution of star-formation-related emission is larger in starbursts and LINERs than in AGNs, this implies that star-formation-related emission gives rise to bluer $L - M'$ colors than do AGNs.

Figure 2 shows the cumulative probability distribution of $L - M'$ colors of type-1 and type-2 AGNs. We apply the Kolmogorov-Smirnov test and find that the probability that the two distributions are drawn from different distributions is 88%. Thus, statistically, the $L - M'$ colors of type-2 AGNs are different from those of type-1 AGNs. However, the difference appears to be very small, the median (mean) being 0.0 (0.2) mag redder in the former than the latter. If the Galactic dust extinction curve ($A_L/A_V = 0.058$, $A_{M'}/A_V = 0.023$; Rieke & Lebofsky 1985) is adopted, the 0.2 mag difference in the $L - M'$ colors implies that type-2 AGNs have higher dust extinction than type-1 AGNs with only $A_V \sim 6$ mag, typically.

We next investigate the “physical” aperture sizes used for the measurements of the $L - M'$ colors of the AGNs, because, when larger physical aperture sizes are used, contamination from extended star-formation-related emission could be larger, which might decrease the $L - M'$ colors. The median physical aperture sizes are 3.0 kpc and 1.3 kpc for type-1 and type-2 AGNs, respectively. Figure 3 compares the cumulative probability distribution of the physical aperture size between type-1 and type-2 AGNs. We do not find any clear trend that physical aperture size is systematically larger for type-2 AGNs than for type-1 AGNs. Furthermore, for type-1 AGNs, the median $L - M'$ colors below and above the median physical aperture size (3.0 kpc) are 0.7 mag and 0.9 mag, respectively. For type-2 AGNs, those below and above the median physical aperture size (1.3 kpc) are 0.9 mag and 1.1 mag, respectively. Therefore, $L - M'$ colors of AGNs measured with larger physical aperture sizes are not systematically bluer due to greater contamination from extended star-formation-related emission. Thus, contamination from extended star-formation-related

emission is unlikely to have strong, systematic effects on the $L - M'$ colors of AGNs.

We next investigate the $L - M'$ colors of type-2 AGNs, distinguishing between those that are less dust-obscured and those highly dust-obscured, because even though a galaxy may be classified as a type-2 AGN, the dust extinction toward its nucleus could vary significantly. For some type-2 AGNs, dust extinction has been estimated to be high. IRAS 08572+3915, NGC 7172, and NGC 7479 display strong silicate dust absorption features at $9.7 \mu\text{m}$ (Dudley & Wynn-Williams 1997, Roche et al. 1991) and strong carbonaceous dust absorption at $3.4 \mu\text{m}$ (Imanishi & Dudley 2000, Imanishi 2000), which means that a large number of both carbonaceous and silicate dust grains lie in front of the background AGN emission. Since interstellar dust consists mainly of carbonaceous and silicate dust grains (Mathis, Rumpl, & Nordsieck 1977, Mathis & Whiffen 1989), the presence of many of these grains along our line of sight to the AGN implies high dust extinction toward the AGN emission. Besides the above sources, a clear $3.4 \mu\text{m}$ carbonaceous dust absorption feature is detected in the spectrum of NGC 1068 (Bridger, Wright & Geballe 1994, Imanishi et al. 1997). For Cygnus A, the observed L -band flux is significantly smaller than that expected from the intrinsic AGN power, which is estimated based on the optical [OIII] flux or extinction corrected 2–10 keV X-ray luminosity (Ward 1996); it is argued that the small L -band flux is a result of flux attenuation by dust extinction (Ward 1996). If the properties of the obscuring dust are similar to those in the Galactic diffuse interstellar medium ($\tau_{3.4}/A_V = 0.004\text{--}0.007$; Pendleton et al. 1994, $\tau_{9.7}/A_V = 0.05\text{--}0.1$; Roche & Aitken 1984, 1985, $A_L/A_V = 0.058$; Rieke & Lebofsky 1985)⁶, then the estimated column density of the obscuring dust is very large, corresponding to $A_V = 140$ mag for Cygnus A (Ward 1996), $A_V > 100$ mag for IRAS 08572+3915 (Imanishi & Ueno 2000), $A_V = 30$ mag for NGC 1068 (Bridger, Wright & Geballe 1994, Imanishi et al. 1997, Marco & Alloin 2000), and $A_V > 20$ mag for NGC 7172 and NGC 7479 (Roche et al. 1991, Imanishi 2000). All of these sources are thus very likely to be highly dust-obscured AGNs.

On the other hand, NGC 2992, IRAS 05189–2524, IRAS 20460+1925, MCG–5–23–16, and PKS 1345+12 show detectable broad $\text{Pa}\alpha$ or $\text{Pa}\beta$ emission lines at $<2 \mu\text{m}$ (Veilleux, Goodrich, & Hill 1997a, Veilleux, Sanders, & Kim 1997b, 1999b). These sources are thus classed as less dust-obscured type-2 AGNs.

In Figure 4 we plot the $L - M'$ colors of these representative samples of less dust-obscured and highly dust-obscured type-2 AGNs. For both less dust-obscured and highly dust-obscured type-2 AGNs, the $L - M'$ colors are similar to the intrinsic $L - M'$

⁶ $\tau_{3.4}$ and $\tau_{9.7}$ mean the optical depths of the $3.4 \mu\text{m}$ carbonaceous dust absorption and the $9.7 \mu\text{m}$ silicate dust absorption, respectively.

color of unobscured AGNs. If the Galactic dust extinction curve of Rieke & Lebofsky (1985) is applied, screen dust extinction with $A_V = 50$ mag should make the $L - M'$ color deviate from the intrinsic color with ~ 1.7 mag. The color deviation in the case of the Galactic dust extinction curve is so large that it should be easily recognizable in the highly dust-obscured type-2 AGNs in Figure 4. The actual color deviation in the highly dust-obscured type-2 AGNs is, however, much smaller than that expected.

Dust obscuration toward type-2 AGNs might be due not only to the dusty tori in the close vicinity of AGNs, but also to dust in the host galaxies (on >100 pc scales). In the latter case, a screen dust extinction model is applicable. Among our five highly dust-obscured AGNs (IRAS 08572+3915, Cygnus A, NGC 1068, NGC 7172, and NGC 7479), NGC 7172 is thought to belong to this class of object (Imanishi 2000). In the former case, where obscuration comes from the torus, the dust has a temperature gradient, with the inner dust having a higher temperature (Pier & Krolik 1992). The L - and M' -band emission is dominated by ~ 900 K and ~ 600 K dust, respectively, and since the M' -band emitting dust is located further out than the L -band emitting dust, M' -band emission suffers less flux attenuation by dust extinction than L -band emission in type-2 AGNs. For IRAS 08572+3915, Cygnus A, NGC 1068, and NGC 7479, since dust extinction toward $3-4 \mu\text{m}$ emission region estimated using $3-4 \mu\text{m}$ data is larger than that toward $\sim 10 \mu\text{m}$ emission region estimated using $\sim 10 \mu\text{m}$ data, and/or that toward $\sim 10 \mu\text{m}$ emission region is larger than that toward $\sim 20 \mu\text{m}$ emission region estimated using $\sim 20 \mu\text{m}$ data, the presence of a temperature gradient in the obscuring dust is strongly suggested, indicating that these objects are obscured by dusty tori (Dudley & Wynn-Williams 1997, Imanishi & Ueno 2000, Imanishi 2000). The presence of this temperature gradient in the obscuring dust should increase (not decrease) the $L - M'$ colors compared to a screen dust extinction model and thus cannot explain the small $L - M'$ colors observed in these highly dust-obscured type-2 AGNs.

5.2. Possible Reasons for the Small $L - M'$ Color Excess in Dust-Obscured AGNs

5.2.1. Time Lag between L - and M' -band Flux Variation

According to the unification paradigm for AGNs, $3-5 \mu\text{m}$ emission is dominated by thermal emission powered by UV to optical emission from the central engine. The UV to optical emission is known to be highly time variable (e.g., Clavel et al. 1992, Nandra et al. 1998). Since the L -band emission region (~ 900 K dust) is located closer to the central engine than the M' -band emission region (~ 600 K dust), a time lag in flux variation is

expected, in the sense that the L -band flux responds to the flux variation of the central UV to optical emission prior to the M' -band flux.

A lower limit on the time lag is determined by the physical separation between the L - and M' -band emission regions. The physical separation depends strongly on the UV to optical luminosity of the central engine and on the assumed dust radial density distribution in the dusty torus. We use the code *DUSTY* (Ivezic, Nenkova, & Elitzur 1999) to estimate the separation in the case of a reasonable dust spatial distribution. *DUSTY* solves the radiative transfer equation for a source embedded in a spherically symmetric dusty envelope and calculates the resulting radial temperature distribution.

We use the same basic parameters for the spectral shape of the central UV to optical emission and the dust composition as those adopted in Imanishi & Ueno (2000), and consider the UV to optical luminosities of central engines with $> 10^{11} L_{\odot}$. We assume the ratio of the outer to inner radius of the dusty envelope to be 200, where the inner radius is determined by the UV to optical luminosity and by the dust sublimation temperature, which is assumed to be ~ 1000 K. Using reasonable parameters, such as a dust extinction toward the central engine of $A_V = 0\text{--}200$ mag and a radial dust density distribution approximated by a power law ($\propto r^{-\gamma}$) with an index of $\gamma = 0\text{--}2$, we find that the physical separation between 900 K and 600 K dust is always larger than a few light days, so the time lag is longer than a few days. The time lag of the flux variation between the L - and M' -band could therefore affect the $L - M'$ color measurements. In fact, the $L - M'$ colors of sources with multiple observations in Tables 2 and 3 are indeed different on different observing dates, and these color differences could be attributed to the time lag. If all the highly dust-obscured type-2 AGNs happened to be observed when they are bright at L but faint at M' , then the derived $L - M'$ colors of these dust-obscured type-2 AGNs would be small. However, although this explanation cannot be ruled out completely, it seems implausible.

5.2.2. Contamination from Compact Nuclear Starbursts

Compact 3–5 μm emission has hitherto been regarded as AGN-related emission. We now consider the possibility that this compact emission may contain a significant contribution from compact nuclear starbursts. The presence of such compact nuclear starbursts has been suggested in some obscured AGNs (e.g., Gonzalez Delgado, Heckman, & Leitherer 2000; but see Ivanov et al. 2000).

If galaxies possessed both AGN and (less obscured) nuclear starburst activity, and if

the intrinsic magnitude ratios of these two components were the same among galaxies, then the contribution of AGN emission to observed 3–5 μm fluxes would be smaller in more highly dust-obscured AGNs as a result of the larger flux attenuation of AGN emission. Thus the $L - M'$ colors would not necessarily be larger in more highly dust-obscured AGNs.

When compact nuclear starbursts contribute significantly to the 3–5 μm fluxes measured within the central few arcsec, the nuclear 3–4 μm spectra are expected to display the 3.3 μm polycyclic aromatic hydrocarbon (PAH) emission (Imanishi & Dudley 2000). However, the nuclear spectra of NGC 1068 ($3''.8 \times 3''.8$), NGC 7172 ($1''.2 \times 5''$), NGC 7479 ($1''.2 \times 5''$), and IRAS 08572+3915 ($1''.2 \times 8''$) show clear 3.4 μm absorption feature but no detectable 3.3 μm PAH emission (Imanishi et al. 1997, Imanishi 2000, Imanishi & Dudley 2000), indicating that the observed 3–4 μm fluxes are dominated by obscured AGN emission and not by starbursts. For Cygnus A, the emission at $>3 \mu\text{m}$ is dominated by nuclear compact emission (Djorgovski et al. 1991, this work, Imanishi & Ueno 2000) and the nuclear spectrum shows no detectable 11.3 μm PAH emission (Imanishi & Ueno 2000), suggesting that in this case too starburst activity contributes little to the observed flux at $>3 \mu\text{m}$. We conclude that for these five highly dust-obscured AGNs (NGC 1068, NGC 7172, NGC 7479, IRAS 08572+3915, and Cygnus A), the small $L - M'$ colors are unlikely to be caused by the contamination from nuclear starburst activity.

5.2.3. Flat Dust Extinction Curve at 3–5 μm

All the above five sources except NGC 7172 are thought obscured by dusty molecular tori in the close vicinity of AGNs (see §5.1). High dust density and high turbulence velocity in these tori could promote dust coagulation (Rossi, Benevides-Soares, & Barbuy 1991), which might make the dust size there much larger than that in the Galactic diffuse interstellar medium (Maiolino et al. 2000a, b). If the size of a typical dust grain in the AGNs' dusty tori is as large as a few μm , as suggested by Maiolino et al. (2000a, b), the extinction curve at 3–5 μm could be much flatter than that in the Galactic diffuse interstellar medium. This flat dust extinction curve at 3–5 μm can explain the small $L - M'$ color excess in the highly dust-obscured AGNs. If this is the case, a strong caveat would need to be attached to estimations of the dust extinction toward AGNs obscured by dusty tori that assume the applicability of a dust extinction curve derived from the Galactic diffuse interstellar medium.

6. Summary

$L - M'$ colors of obscured and unobscured AGNs were investigated. The $L - M'$ color excess in highly dust-obscured AGNs due to dust extinction, when compared to less dust-obscured AGNs, was much smaller than that expected from the Galactic dust extinction curve. We argued that the size of the dust grains in the close vicinity of AGNs may be so large, due to coagulation, that the extinction curve at 3–5 μm is flatter than that in the Galactic diffuse interstellar medium.

We thank P. Fukumura-Sawada, D. Griep and C. Kaminski for their support during the IRTF run. We are grateful to Drs. J. Rayner and W. Vacca for their kind instruction how to use NSFCAM prior to actual observing runs, and to Dr. R. Nakamura for useful discussion about dust coagulation processes. Drs. T. Nakajima, C. C. Dudley, and the anonymous referee gave useful comments on this manuscript. MI was financially supported by the Japan Society for the Promotion of Science for his stays at the University of Hawaii. Drs. A. T. Tokunaga and H. Ando gave MI the opportunity to work at the University of Hawaii. This research has made use of the NASA/IPAC Extragalactic Database (NED) which is operated by the Jet Propulsion Laboratory, California Institute of Technology, under contract with the National Aeronautics and Space Administration.

REFERENCES

- Alonso-Herrero, A., Ward, M. J., & Kotilainen, J. K. 1997, *MNRAS*, 288, 977
- Alonso-Herrero, A., Simpson, C., Ward, M. J., & Wilson, A. S. 1998, *ApJ*, 495, 196
- Alonso-Herrero, A., Quillen, A. C., Simpson, C., Efstathiou, A., & Ward, M. J. 2000, *AJ*, in press (astro-ph/0012096)
- Antonucci, R. 1993, *ARA&A*, 31, 473
- Becklin, E. E., Tokunaga, A. T., & Wynn-Williams, C. G. 1982, *ApJ*, 263, 624
- Bridger, A., Wright, C. S., & Geballe, T. R. 1994, *Infrared Astronomy with Arrays: the Next Generation*, I. McLean ed. (Dordrecht: Kluwer Academic Publishers), p. 537
- Clavel, J. et al. 1992, *ApJ*, 393, 113
- Djorgovski, S., Weir, N., Matthews, K., & Graham, J. R. 1991, *ApJ*, 372, L67
- Dudley, C. C. 1998, Ph. D. Thesis, University of Hawaii
- Dudley, C. C., & Wynn-Williams C. G. 1997, *ApJ*, 488, 720
- Elvis, M., Willner, S. P., Fabbiano, G., Carleton, N. P., Lawrence, A., & Ward, M. 1984, *ApJ*, 280, 574
- Gonzalez Delgado, R. M., Heckman, T., & Leitherer, C. 2000, *ApJ*, in press, (astro-ph/0008417)
- Halpern, J. P., Turner, T. J., & George, I. M. 1999, *MNRAS*, 307, L47
- Heckman, T. M., Smith, E. P., Baum, S. A., van Breugel, W. J. M., Miley, G. K., Illingworth, G. D., Bothun, G. D., & Balick, B. 1986, *ApJ*, 311, 526
- Imanishi, M. 2000, *MNRAS*, 319, 331
- Imanishi, M., & Dudley, C. C. 2000, *ApJ*, 545, 701
- Imanishi, M., & Ueno, S. 2000, *ApJ*, 535, 626
- Imanishi, M., Terada, H., Sugiyama, K., Motohara, K., Goto, M., & Maihara, T. 1997, *PASJ*, 49, 69
- Ivanov, V. D., Rieke, G. H., Groppi, C. E., Alonso-Herrero, A., Rieke, M. J., & Engelbracht, C. W. 2000, *ApJ*, in press, (astro-ph/0007177)

- Ivezic, Z., Nenkova, M., & Elitzur, M. 1999, User Manual for DUSTY, University of Kentucky Internal Report, accessible at [http://www.pa.uky.edu/~moche/dusty/\(astro-ph/9910475\)](http://www.pa.uky.edu/~moche/dusty/(astro-ph/9910475))
- Jackson, N., & Rawlings, S. 1997, MNRAS, 286, 241
- Lawrence, A., Ward, M., Elvis, M., Fabbiano, G., Willner, S. P., Carleton, N. P., & Longmore, A. 1985, 291, 117
- Lutz, D., et al. 1996, A&A, 315, L269
- Maiolino, R., Marconi, A., & Oliva, E. 2000a, A&A, in press, (astro-ph/0010066)
- Maiolino, R., Marconi, A., Salvati, M., Risaliti, G., Severgnini, P., Oliva, E., La Franca, F., & Vanzì, L. 2000b, A&A, in press, (astro-ph/0010009)
- Marco, O., & Alloin, D. 2000, A&A, 353, 465
- Mathis, J. S., & Whiffen, G. 1989, ApJ, 341, 808
- Mathis, J. S., Rumpl, W., & Nordsieck, K. H. 1977, ApJ, 217, 425
- McAlary, C. W., McLaren, R. A., & Crabtree, D. R. 1979, ApJ, 234, 471
- McAlary, C. W., McLaren, R. A., & McGonegal, R. J. 1983, ApJS, 52, 341
- Moorwood, A. F. M., & Glass, I. S. 1984, A&A, 135, 281
- Nandra, K., & Pounds, K. A. 1994, MNRAS, 268, 405
- Nandra, K., Clavel, J., Edelson, R. A., George, I. M., Malkan, M. A., Mushotzky, R. F., Peterson, B. M., & Turner, T. J. 1998, ApJ, 505, 594
- Neugebauer, G., Green, R. F., Matthews, K., Schmidt, M., Soifer, B. T., & Bennett, J. 1987, ApJS, 63, 615
- Osterbrock, D. E. 1983, PASP, 95, 12
- Osterbrock, D. E., & Miller, J. S. 1975, ApJ, 197, 535
- Pendleton, Y. J., Sandford, S. A., Allamandola, L. J., Tielens, A. G. G. M., & Sellgren, K. 1994, ApJ, 437, 683
- Pier, E. A., & Krolik, J. H. 1992, ApJ, 401, 99

- Rieke, G. H., & Lebofsky M. J. 1985, ApJ, 288, 618
- Roche, P. F., & Aitken, D. K. 1984, MNRAS, 208, 481
- Roche, P. F., & Aitken, D. K. 1985, MNRAS, 215, 425
- Roche, P. F., Aitken, D. K., Smith, C. H., & Ward, M. J. 1991, MNRAS, 1991, 248, 606
- Rossi, S. C. F., Benevides-Soares, P., & Barbuy, B. 1991, A&A, 251, 587
- Rush, B., Malkan, M. A., & Spinoglio, L. 1993, ApJS, 89, 1
- Scoville, N. Z., et al. 2000, AJ, 119, 991
- Shure, M. A., Toomey, D. W., Rayner, J. T., Onaka, P., & Denault, A. J. 1994, Proc. SPIE, 2198, 614
- Simpson, C. 1998a, ApJ, 509, 653
- Simpson, C. 1998b, MNRAS, 297, L39
- Simpson, C., Rawlings, S., & Lacy, M. 1999, MNRAS, 306, 828
- Simpson, C., Ward, M., & Wall, J. V. 2000, MNRAS, 319, 963
- Smith, D. A., & Done, C. 1996, MNRAS, 280, 355
- Tadhunter, C. N., Morganti, R., Robinson, A., Dickson, R., Villar-Martin, M., & Fosbury, R. A. E. 1998, MNRAS, 298, 1035
- Vader, J. P., Frogel, J. A., Terndrup, D. M., & Heisler, C. A. 1993, AJ, 106, 1743
- Veilleux, S., Kim, D. -C., Sanders, D. B., Mazzarella, J. M., & Soifer, B. T. 1995, ApJS, 98, 171
- Veilleux, S., Goodrich, R. W., & Hill, G. J. 1997a, ApJ, 477, 631
- Veilleux, S., Kim, D. -C., & Sanders, D. B. 1999a, ApJ, 522, 113
- Veilleux, S., Sanders, D. B., & Kim, D. -C. 1997b, ApJ, 484, 92
- Veilleux, S., Sanders, D. B., & Kim, D. -C. 1999b, ApJ, 522, 139
- Ward, M. J. 1996, in Cygnus A - Study of a Radio Galaxy, Carilli, C. L., & Harris, D. E., eds, Cambridge University Press, p.43

Ward, M., Elvis, M., Fabbiano, G., Carleton, N. P., Willner, S. P., & Lawrence, A. 1987, ApJ, 315, 74

Xu, C., Livio, M., & Baum, S. 1999, AJ, 118, 1169

Young, S., Axon, D. J., Hough, J. H., Fabian, A. C., & Ward, M. J. 1998, MNRAS, 294, 478

Table 1. Observing Log

Object (1)	redshift (2)	$L[\text{OIII}]$ (10^{42} erg s $^{-1}$) (3)	Integration Time (sec)		Observing Date (UT)	
			L (4)	M' (5)	L (6)	M' (7)
3C 63	0.175	2 ^a	1000	1200	1999 Nov 29	1999 Nov 29
3C 171	0.238	5 ^a	1800	3600	1999 Nov 28	1999 Nov 29
3C 195 (0806–10)	0.110	5 ^b	900	1200	1999 Nov 28	1999 Nov 29
3C 234	0.184	21 ^a	400	800	1999 Nov 29	1999 Nov 29
			200	400	2000 May 16	2000 May 16
3C 321	0.096	2 ^a	400	1600	2000 May 15	2000 May 15
			400	1800	2000 May 16	2000 May 16
3C 445	0.056	1 ^a	200	400	2000 May 15	2000 May 15
3C 456	0.233	6 ^a	1200	2400	1999 Nov 28	1999 Nov 29
Cygnus A	0.056	1 ^c	600	2400	2000 Apr 19	2000 Apr 19
			400	1800	2000 May 16	2000 May 16
Mrk 231	0.042	1 ^d	150	200	2000 Apr 18	2000 Apr 18
PG 1534+580 (Mrk 290)	0.032	1 ^d	300	800	2000 Apr 19	2000 Apr 19
PKS 1345+12	0.122	2 ^d	600	800	2000 Apr 19	2000 Apr 19

Note. — Column (1): Object name. Column (2): Redshift. Column (3): Optical [OIII] emission line luminosity in 10^{42} erg s $^{-1}$ and references. ^a: Jackson & Rawlings 1997; ^b: Tadhunter et al. 1998; ^c: Osterbrock & Miller 1975; ^d: Xu, Livio, & Baum 1999. Columns (4) and (5): Net on source integration time for L - and M' -band photometry in seconds, respectively. Columns (6) and (7): Observing date for L - and M' -band photometry in UT, respectively.

Table 2. Photometric Results

Object	L	M'	$L - M'$	Aperture arcsec (kpc)	Type
(1)	(2)	(3)	(4)	(5)	(6)
3C 63	13.4±0.3	>11.0	<2.7	6 (16.6)	Sy2 ^a
3C 171	>13.9	>10.9	...	6 (21.1)	Sy2 ^a
3C 195	10.7±0.1	9.9±0.1	0.8±0.1	6 (11.2)	Sy2 ^b
3C 234	10.7±0.1	9.5±0.2	1.2±0.2	6 (17.3)	Sy2 ^c
	10.6±0.1	9.3±0.2	1.3±0.2	6 (17.3)	...
3C 321 *	12.5±0.1	11.7±0.3	0.8±0.3	6 (10.0)	Sy2 ^a
	12.5±0.1	11.4±0.2	1.1±0.2	6 (10.0)	...
3C 445	9.2±0.1	8.4±0.1	0.8±0.1	6 (6.1)	Sy1 ^a
3C 456	12.7±0.2	>10.1	<2.8	6 (20.8)	Sy2 ^a
Cygnus A	12.7±0.1	11.4±0.3	1.3±0.3	6 (6.1)	Sy2 ^d
	12.0±0.1	11.1±0.2	0.9±0.2	6 (6.1)	...
Mrk 231	7.4±0.1	6.4±0.1	1.0±0.1	6 (4.7)	Sy1 ^e
PG 1534+580	10.9±0.1	10.3±0.3	0.6±0.3	6 (3.6)	Sy1 ^f
PKS 1345+12 *	11.5±0.1	10.7±0.2	0.8±0.2	6 (12.3)	Sy2 ^e

Note. — Column (1): Object name. Column (2): L -band magnitude. When sources are observed twice, both photometric results are shown as independent data instead of combining these data, to see time variation. Column (3): M' -band magnitude. Column (4): $L - M'$ color in magnitude. Column (5): Aperture size in arcsec used for the photometry. Corresponding physical size in kpc is also shown in parentheses. Column (6): Optical spectral type and references. Sy1 : type-1 AGNs. Sy2 : type-2 AGNs. ^a: Jackson & Rawlings 1997; ^b: Tadhunter et al. 1998; ^c: Young et al. 1998; ^d: Osterbrock 1983; ^e: Veilleux, Kim, & Sanders 1999a; ^f: Xu, Livio, & Baum 1999. Although 3C 234 shows broad optical emission lines, we classified this source as Sy2 following the reference.

*: 3C 321 and PKS 1345+12 have double nuclei with separations of a few arcsec (Heckman et al. 1986, Scoville et al. 2000), but the L - and M' -band fluxes of each object come predominantly from the main nucleus.

Table 3. 3–5 μm Photometric Results in the Literature.

Type	Object	Redshift	L	M'	$L - M'$	Aperture arcsec (kpc)	Reference
(1)	(2)	(3)	(4)	(5)	(6)	(7)	(8)
Sy 1	NGC 863 (Mrk 590)	0.026	9.3	8.5	0.8	8, 5 (3.9, 2.5)	1
	NGC 931 (Mrk 1040)	0.017	8.4	7.6	0.8	8, 5 (2.6, 1.6)	1
			8.9 \pm 0.1	7.9 \pm 0.2	1.0 \pm 0.2	7.9 (2.6)	2
	NGC 1365	0.005	7.6 \pm 0.1	6.9 \pm 0.1	0.7 \pm 0.1	9.1 (0.9)	2
			7.6 \pm 0.1	7.0 \pm 0.1	0.6 \pm 0.1	5 (0.5)	3
	NGC 3227	0.004	8.9 \pm 0.1	8.4 \pm 0.5	0.5 \pm 0.5	4.6 (0.4)	2
			8.6 \pm 0.1	8.0	0.6	15 (1.2)	4
	NGC 3516	0.009	8.4 \pm 0.1	8.1 \pm 0.6	0.3 \pm 0.6	15, 10 (2.6, 1.7)	4
	NGC 4051	0.002	9.0 \pm 0.1	8.0	1.0	15 (0.6)	4
	NGC 4151	0.003	7.4 \pm 0.1	6.4 \pm 0.1	1.0 \pm 0.1	7.9 (0.5)	2
			7.3 \pm 0.1	6.4 \pm 0.1	0.9 \pm 0.1	10 (0.6)	4
	NGC 5548	0.017	8.6 \pm 0.1	8.0 \pm 0.3	0.6 \pm 0.3	7.9 (2.6)	2
			9.0 \pm 0.1	8.0 \pm 0.7	1.0 \pm 0.7	10 (3.2)	4
	NGC 6814	0.005	9.8 \pm 0.1	8.9 \pm 0.6	0.9 \pm 0.6	7.9 (0.8)	2
	NGC 7469	0.016	8.1 \pm 0.1	7.0 \pm 0.2	1.1 \pm 0.2	7.9 (2.4)	2
			8.0 \pm 0.1	7.4 \pm 0.1	0.6 \pm 0.1	5 (1.5)	3
	3A 0557–385	0.034	8.3	7.1	1.2	5 (3.2)	1
	3C 120	0.033	9.2 \pm 0.1	8.4 \pm 0.7	0.8 \pm 0.7	15 (9.2)	4
	3C 273	0.158	8.0 \pm 0.1	7.3 \pm 0.2	0.7 \pm 0.2	9.1 (23.2)	2
	3C 445	0.056	9.5	8.6	0.9	8, 5 (8.1, 5.1)	5
	Akn 120	0.032	9.0 \pm 0.1	8.1 \pm 0.3	0.9 \pm 0.3	4.6 (2.8)	2
	ESO 113–IG45	0.045	8.4 \pm 0.1	8.1 \pm 0.3	0.3 \pm 0.3	9.1 (7.5)	2
	IC 4329A	0.016	7.8 \pm 0.1	7.5 \pm 0.1	0.3 \pm 0.1	4.6 (1.4)	2
			7.9 \pm 0.1	6.9 \pm 0.3	1.0 \pm 0.3	15 (4.6)	4
	MCG–2–58–22	0.048	9.3	8.6	0.7	8, 5 (7.0, 4.4)	1
	MCG 8–11–11	0.020	8.9	7.9	1.0	8, 5 (3.0, 1.9)	1
		8.8 \pm 0.1	8.1 \pm 0.3	0.7 \pm 0.3	7.9 (3.0)	2	
		8.8 \pm 0.1	7.3 \pm 0.2	1.5 \pm 0.2	15 (5.7)	4	
Mrk 79	0.022	9.3	8.4	0.9	8 (3.3)	1	
Mrk 231	0.042	7.4 \pm 0.1	6.5 \pm 0.1	0.9 \pm 0.1	10 (7.8)	4	
Mrk 335	0.026	8.7 \pm 0.1	7.6 \pm 0.2	1.1 \pm 0.2	7.9 (3.9)	2	
Mrk 359	0.017	10.3 \pm 0.1	9.2 \pm 0.1	1.1 \pm 0.1	5 (1.6)	6	
Mrk 1152	0.053	10.6	9.4	1.2	8, 5 (7.7, 4.8)	1	
Sy 2	NGC 262 (Mrk 348)	0.015	10.5 \pm 0.1	9.1 \pm 0.1	1.4 \pm 0.1	3 (0.9)	7
	NGC 526a	0.019	9.6	8.4	1.2	8, 5 (2.9, 1.8)	1
	NGC 1052	0.005	9.8 \pm 0.1	9.1 \pm 0.2	0.7 \pm 0.2	3 (0.3)	7
			9.7 \pm 0.1	9.3 \pm 0.2	0.4 \pm 0.2	4 (0.4)	8

Table 3—Continued

Type	Object	Redshift	L	M'	$L - M'$	Aperture arcsec (kpc)	Reference
(1)	(2)	(3)	(4)	(5)	(6)	(7)	(8)
	NGC 1068	0.004	5.3	3.7	1.6±0.4	0.6 (0.1)	9
			4.5±0.1	3.2±0.1	1.3±0.1	3 (0.2)	7
	NGC 1275	0.018	8.1±0.1	7.1±0.1	1.0±0.1	7.9 (2.7)	2
	NGC 1808	0.003	8.7±0.1	8.7±0.2	0.0±0.2	5 (0.3)	3
	NGC 2992	0.008	9.2	8.4	0.8	6 (0.9)	1
			10.0±0.1	9.2±0.3	0.8±0.3	3 (0.5)	7
	NGC 3094	0.008	8.2±0.1	7.5±0.1	0.7±0.1	5 (0.8)	3
	NGC 3281	0.011	8.4	7.2	1.2	6 (1.3)	10
	NGC 4418 ^a	0.007	11.1±0.1	10.2±0.2	0.9±0.2	5 (0.7)	3
	NGC 4736	0.001	7.0±0.1	7.4±0.4	−0.4±0.4	15 (0.3)	4
	NGC 4945	0.002	8.3	7.5	0.8	7.5 (0.3)	11
	NGC 4968	0.010	10.0±0.1	8.7±0.2	1.3±0.2	3 (0.6)	7
	NGC 5252	0.023	10.6±0.1	10.0±0.3	0.6±0.3	3 (1.3)	7
	NGC 5506	0.006	7.6±0.1	6.7±0.1	0.9±0.1	4.6 (0.5)	2
			7.1±0.1	6.2±0.1	0.9±0.1	3 (0.4)	7
	NGC 7130 (IC 5135)	0.016	10.0±0.1	9.9±0.2	0.1±0.2	7.8 (2.4)	3
	NGC 7172	0.009	9.1±0.1	8.5±0.1	0.6±0.1	5 (0.9)	3
			8.2	7.3±0.1	0.9±0.1	8, 5 (1.4, 0.9)	6
			9.5±0.1	8.6±0.1	0.9±0.1	3 (0.5)	7
	NGC 7314	0.005	10.3	9.4	0.9	5 (0.5)	1
	NGC 7479	0.008	9.8±0.1	8.6±0.1	1.2±0.1	5 (0.8)	3
	NGC 7582	0.005	7.8±0.1	7.1±0.1	0.7±0.1	9.1 (0.9)	2
	NGC 7674 (Mrk 533)	0.029	9.0±0.1	8.2±0.1	0.8±0.1	5 (2.7)	3
			9.1±0.1	8.0±0.1	1.1±0.1	3 (1.6)	7
	3C 33	0.060	11.9±0.1	11.2±0.1	0.7±0.1	3 (3.3)	12
	3C 223	0.137	12.9±0.1	11.8±0.2	1.1±0.2	3 (6.8)	12
	3C 234	0.185	10.9	9.3	1.6	6 (17.4)	5
			10.5±0.1	9.9±0.1	0.6±0.1	3 (8.7)	12
	Circinus	0.002	6.4	5.1	1.3	5 (0.2)	11
	IRAS 00198–7926	0.073	9.8	7.7	2.1	4.7 (6.1)	13
	IRAS 00521–7054	0.069	9.2	8.1	1.1	6.2 (7.6)	13
	IRAS 04385–0828	0.015	9.5	8.0	1.5	4.7 (1.3)	13
	IRAS 05189–2524	0.042	8.1±0.1	7.4±0.1	0.7±0.1	5 (3.9)	3
			8.5	7.2	1.3	4.7 (3.6)	13
	IRAS 08572+3915 ^b	0.058	9.2±0.3	8.0±0.3	1.2±0.4	4.5 (4.7)	14
	IRAS 20460+1925	0.181	9.2	8.3	0.9	11.9 (33.9)	13
	MCG–5–23–16	0.008	8.5±0.1	7.7±0.1	0.8±0.1	3 (0.5)	7
	Mrk 573	0.017	10.1±0.1	9.0±0.3	1.1±0.3	3 (1.0)	7

Table 3—Continued

Type	Object	Redshift	L	M'	$L - M'$	Aperture arcsec (kpc)	Reference
(1)	(2)	(3)	(4)	(5)	(6)	(7)	(8)
SB	NGC 520	0.008	9.6±0.1	9.1±0.2	0.5±0.2	7.8 (1.2)	3
LINER	NGC 613	0.005	9.5±0.1	8.7±0.1	0.8±0.1	5 (0.5)	3
Unknown	NGC 660	0.003	8.9±0.1	8.7±0.1	0.2±0.1	5 (0.3)	3
	NGC 828	0.018	10.4±0.1	10.6±0.1	-0.2±0.1	5 (1.7)	3
	NGC 1614 (Mrk 617)	0.016	9.0±0.1	8.6±0.1	0.4±0.1	7.8 (2.4)	3
			9.2	8.8±0.1	0.4±0.1	5 (1.5)	6
	NGC 2110	0.008	9.4	8.9±0.2	0.5±0.2	6 (0.9)	6
	NGC 2339	0.007	9.7±0.1	9.5±0.2	0.2±0.2	7.8 (1.1)	3
	NGC 2388	0.014	10.1±0.1	9.8±0.2	0.3±0.2	5 (1.3)	3
	NGC 2623	0.018	10.6±0.1	10.2±0.2	0.4±0.2	5 (1.7)	3
	NGC 2782	0.009	10.1±0.1	9.6±0.1	0.5±0.1	5 (0.9)	3
	NGC 3079	0.004	9.2	9.4±0.2	-0.2±0.2	6 (0.5)	6
	NGC 4102	0.003	8.5±0.1	8.3±0.1	0.2±0.1	5 (0.3)	3
	NGC 4194 (Mrk 201)	0.008	9.4±0.1	8.9±0.1	0.5±0.1	5 (0.8)	3
	NGC 4579	0.005	9.4	9.5±0.3	-0.1±0.3	6 (0.6)	6
	NGC 4826	0.001	8.9	9.2±0.2	-0.3±0.2	6 (0.1)	6
	NGC 6764	0.008	10.9	9.9±0.2	1.0±0.2	5 (0.8)	6
	NGC 7714	0.009	10.4±0.1	10.1±0.2	0.3±0.2	5 (0.9)	3
	NGC 7770	0.014	11.2±0.1	10.5±0.2	0.7±0.2	5 (1.3)	3
	NGC 7771	0.014	10.3±0.1	9.9±0.1	0.4±0.1	5 (1.3)	3
	MCG-3-4-14	0.033	10.7±0.1	10.2±0.2	0.5±0.2	5 (3.1)	3
	Mrk 331	0.018	9.8±0.1	9.5±0.2	0.3±0.2	5 (1.7)	3
	UGC 3094	0.025	10.6±0.1	10.2±0.2	0.4±0.2	5 (2.4)	3

Note. — Column (1): Spectral type. Sy1: type-1 AGNs. Sy2: Dust-obscured AGNs either based on optical spectral type or detailed studies at other wavelengths. SB: starburst galaxies. LINER: LINER-type galaxies. Column (2): Object name. Column (3): Redshift. Column (4): L - or L' -band magnitude. Column (5): M' - or M -band magnitude. Column (6): $L - M'$ color in magnitude. Column (7): Aperture size in arcsec and corresponding physical size in kpc (in parentheses) used for the photometry. Column (8): Reference for the photometry. 1: Ward et al. 1987; 2: McAlary, McLaren, & McGonegal 1983; 3: Dudley 1998; 4: McAlary, McLaren, & Crabtree 1979; 5: Elvis et al. 1984; 6: Lawrence et al. 1985; 7: Alonso-Herrero et al. 2000; 8: Becklin, Tokunaga, & Wynn-Williams 1982; 9: Marco & Alloin 2000; 10: Simpson 1998a; 11: Moorwood & Glass 1984; 12: Simpson et al. 2000; 13: Vader et al. 1993; 14: Dudley & Wynn-Williams 1997.

^a: Although NGC 4418 is optically a normal star-forming galaxy (Rush, Malkan, & Spinoglio 1993), we classify this source as a Sy 2 based on a detailed infrared study by Dudley & Wynn-Williams (1997).

^b: Although IRAS 08572+3915 is optically a LINER (Veilleux et al. 1995), we classify this source as a Sy 2 based on detailed infrared studies by Dudley & Wynn-Williams (1997) and Imanishi & Ueno (2000).

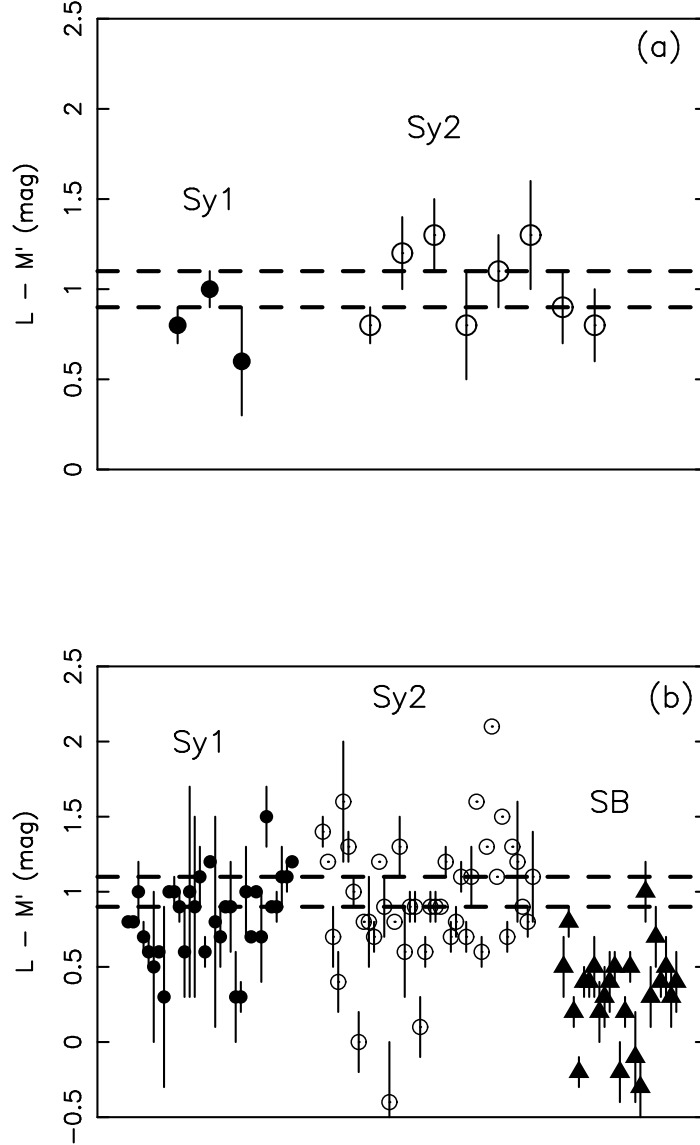


Fig. 1.— (a): Distribution of $L - M'$ colors of type-1 and type-2 AGNs that we observed (Table 2). Filled circles: type-1 AGNs. Open circles: type-2 AGNs. The region between the two dashed lines denotes the intrinsic $L - M'$ color ($= 1.0 \pm 0.1$) of AGNs in the case of no dust extinction (see § 4). 3C 234, 3C 321, and Cygnus A were observed twice, and these two data points are plotted independently. 3C 63, 3C 171, and 3C 456 are excluded because their $L - M'$ colors were not derived directly from the observed data. (b) $L - M'$ colors of AGNs and starburst/LINER galaxies taken from the literature (Table 3). Filled circles: type-1 AGNs. Open circles: type-2 AGNs. Filled triangles: starbursts, LINERs and galaxies with unknown spectral type. The region between the two dashed lines denotes the intrinsic $L - M'$ ($= 1.0 \pm 0.1$) color of AGNs in the case of no dust extinction (see § 4).

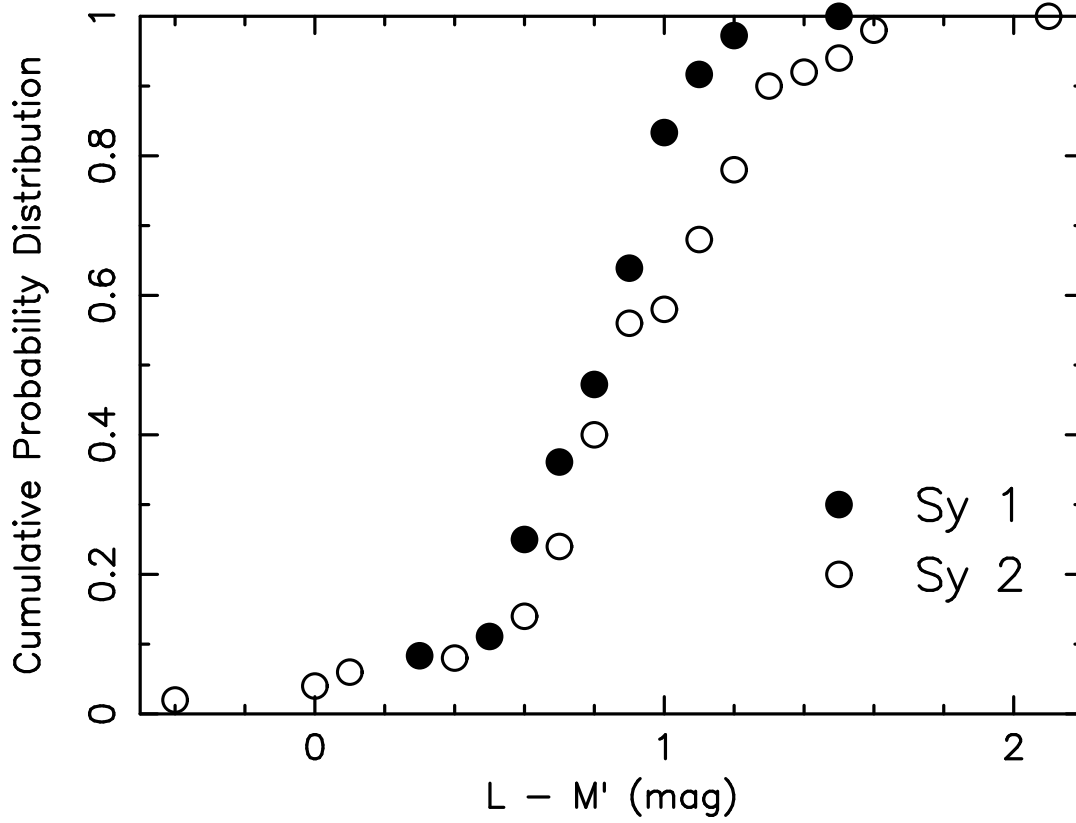


Fig. 2.— Cumulative probability distribution of $L - M'$ colors. Filled circles: type-1 AGNs (36 data points). Open circles: type-2 AGNs (50 data points).

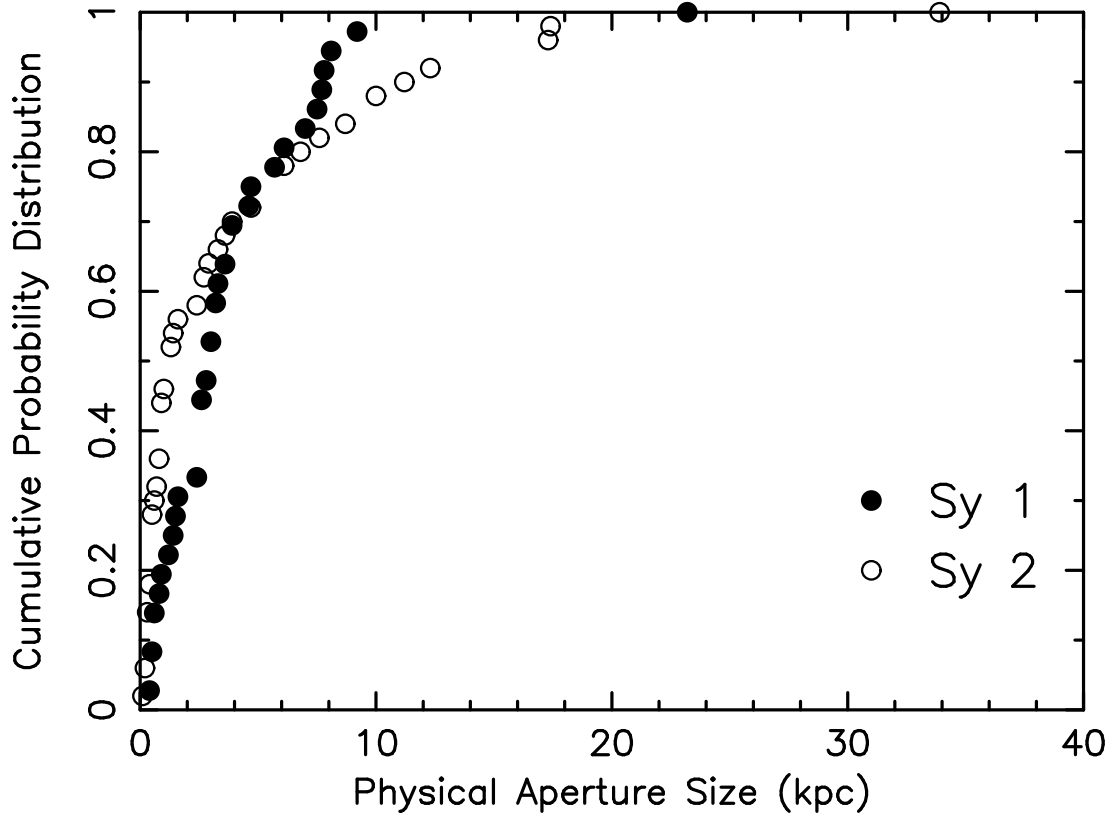


Fig. 3.— Cumulative probability distribution of physical aperture size in kpc. Filled circles: type-1 AGNs. Open circles: type-2 AGNs.

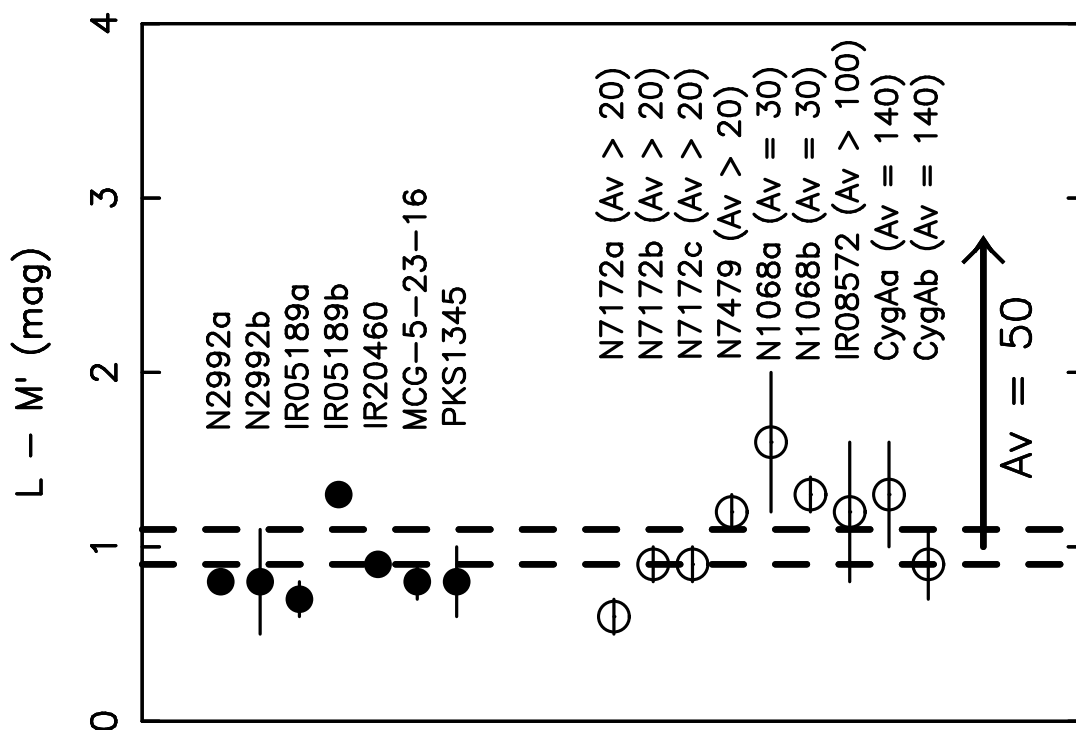


Fig. 4.— $L - M'$ colors of the representative samples of type-2 AGNs. Filled circles: less obscured type-2 AGNs for which broad $\text{Pa}\alpha$ or $\text{Pa}\beta$ emission components are detected at $< 2 \mu\text{m}$. Open circles: highly dust-obscured type-2 AGNs. Estimated A_V values are shown in the figure. See the text (§ 5.1) for more details. The length of the upper arrow corresponds to the $L - M'$ color excess by dust extinction with $A_V = 50$ mag for the Galactic dust extinction curve.